Supporting Information

Highly Aligned Aramid Nanofibrillar Nanocomposites for Enhanced Dynamic Mechanical Properties

Donggeun Lee[1], *Jinhan Cho*[2,3], *Jeong Gon Son*[3,4], *Bongjun Yeom*[1]*

[1]Department of Chemical Engineering, Hanyang University, Seoul 04763, Republic of Korea

[2]Department of Chemical and Biological Engineering, Korea University, Seoul 02841, Republic of Korea

[3]KU-KIST Graduate School of Converging Science and Technology, Korea University, Seoul 02841, Republic of Korea

[4]Soft Hybrid Materials Research Center, Korea Institute of Science and Technology (KIST), Seoul 02792, Republic of Korea

Table S1. Summary of PVA α or/and ANF β* relaxation temperature for PVA, ANF and ANF/PVA nanocomposites. (The relaxation temperatures were designated to the temperatures at the peak positions in the range of 100-200 ºC)

	PVA α or/and ANF β* relaxation temperature [ºC]
PVA	104.4
ANP35	142.8
S-ANP35 0º	168.3
S-ANP35 45º	167.8
S-ANP35 90º	167.7
ANP48	160.7
S-ANP48 0º	175.0
S-ANP48 45º	177.5
S-ANP48 90º	176.5
ANF	202.9

Table S2. Dynamic mechanical results at 30 Hz of PVA and ANF/PVA nanocomposites with various volume fractions and loading

	Storage modulus [GPa]	tanδ	$(E^*/\rho)\cdot(\tan\delta)^{0.5}$ [10^6 m^2/s^2]
PVA	3.2 ± 0.3	0.100 ± 0.008	0.78 ± 0.05
S-PVA 0º	5.1 ± 0.4	0.092 ± 0.013	1.18 ± 0.11
S-PVA 45º	3.8 ± 0.7	0.077 ± 0.003	0.81 ± 0.15
S-PVA 90º	3.0 ± 0.3	0.079 ± 0.007	0.66 ± 0.07
ANP35	4.4 ± 0.3	0.125 ± 0.004	1.16 ± 0.08
S-ANP35 0º	10.8 ± 1.5	0.057 ± 0.008	1.91 ± 0.36
S-ANP35 45º	4.6 ± 0.7	0.070 ± 0.001	0.92 ± 0.14
S-ANP35 90º	4.2 ± 0.3	0.067 ± 0.004	0.81 ± 0.07
ANP48	5.8 ± 0.9	0.105 ± 0.014	1.37 ± 0.16
S-ANP48 0º	13.6 ± 1.2	0.060 ± 0.005	2.43 ± 0.20
S-ANP48 45º	6.9 ± 0.9	0.072 ± 0.004	1.35 ± 0.13
S-ANP48 90º	6.6 ± 1.0	0.076 ± 0.006	1.33 ± 0.22

Table S3. Summary of dynamic mechanical properties obtained at 1 Hz for PVA, ANP35 and S-ANP35 0º with different relative humidity conditions.

	Storage modulus [GPa]	tanδ	$(E^*/\rho)\cdot(\tan\delta)^{0.5}$ [10^6 m^2/s^2]
PVA at 43% RH	2.6	0.088	0.60
PVA at 84% RH	0.15	0.350	0.07
ANP35 at 43% RH	3.4	0.143	0.97
ANP35 at 84% RH	1.7	0.261	0.63
S-ANP35 0º at 43% RH	9.5	0.065	1.80
S-ANP35 0º at 84% RH	2.9	0.129	0.78

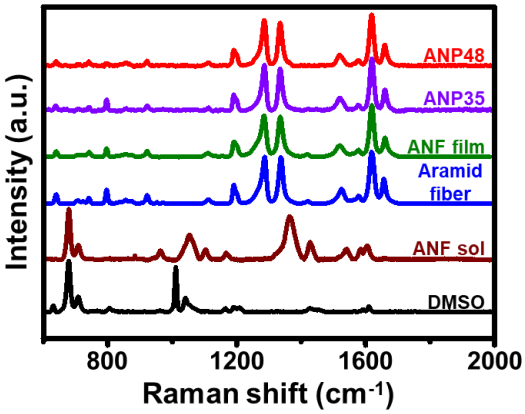

Figure S1. Raman scattering spectra of DMSO, ANF solution, aramid fiber, ANF film, and ANF/PVA nanocomposites with different volume fractions of fillers.

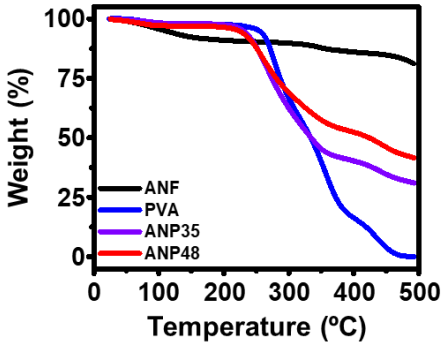

Figure S2. Thermogravimetric analysis data for ANF, PVA, and ANF/PVA nanocomposites. Pristine ANF exhibited outstanding thermal properties, with a mass loss of about 20% even when heated to 500 ºC. Degradation of PVA starts at 250 ºC and no residues are left after heating to 500 ºC. Degradation of ANP35 and ANP48 starts at 220 ºC, and leaves 30%, 41% of residues after heating to 500 ºC, respectively.

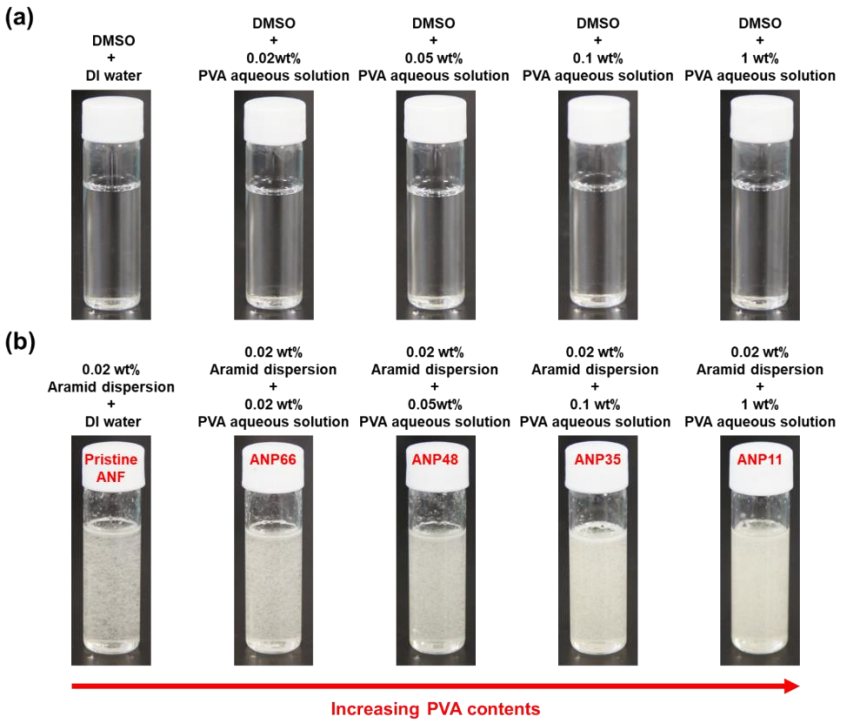

Figure S3. Photographs of mixtures water or PVA aqueous solution with (a) DMSO and (b) 0.02 wt% aramid nanoseed dispersion, with a volume ratio of 9:10. Concentrations of PVA aqueous solution varies from 0.02 wt% to 1wt%.

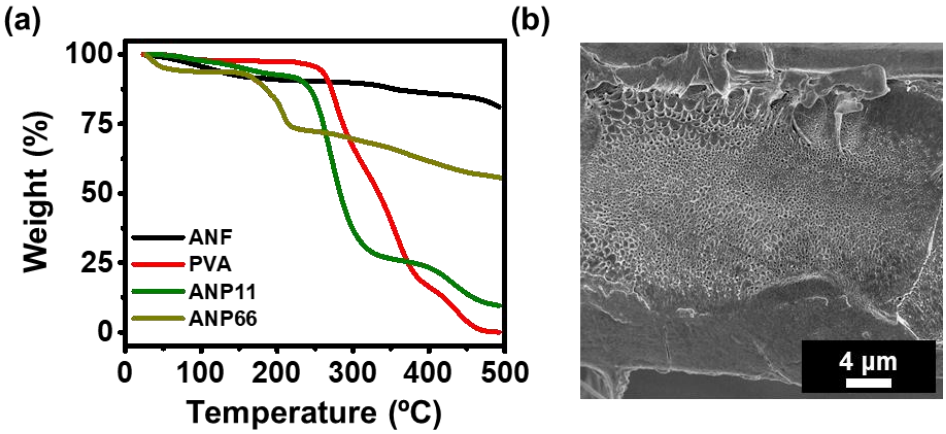

Figure S4. (a) Thermogravimetric analysis for ANP 11 and ANP 66 nanocomposites. (b) Cross-sectional FE-SEM image of ANP11 sample. Large volume fraction of PVA leaded uneven distributions of ANF. ANP66 samples were too brittle for mechanical tests.

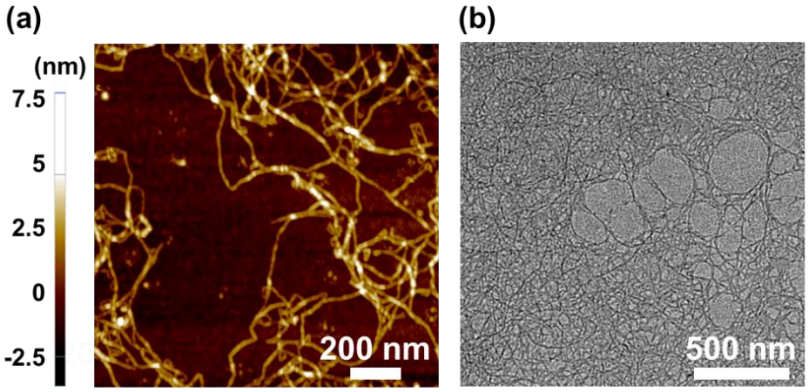

Figure S5. (a) AFM and (b) TEM images of pristine ANF.

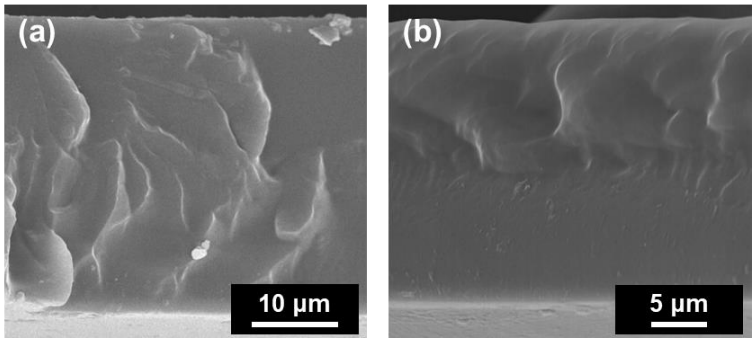

Figure S6. FE-SEM cross-sectional images of (a) PVA, (b) S-PVA.

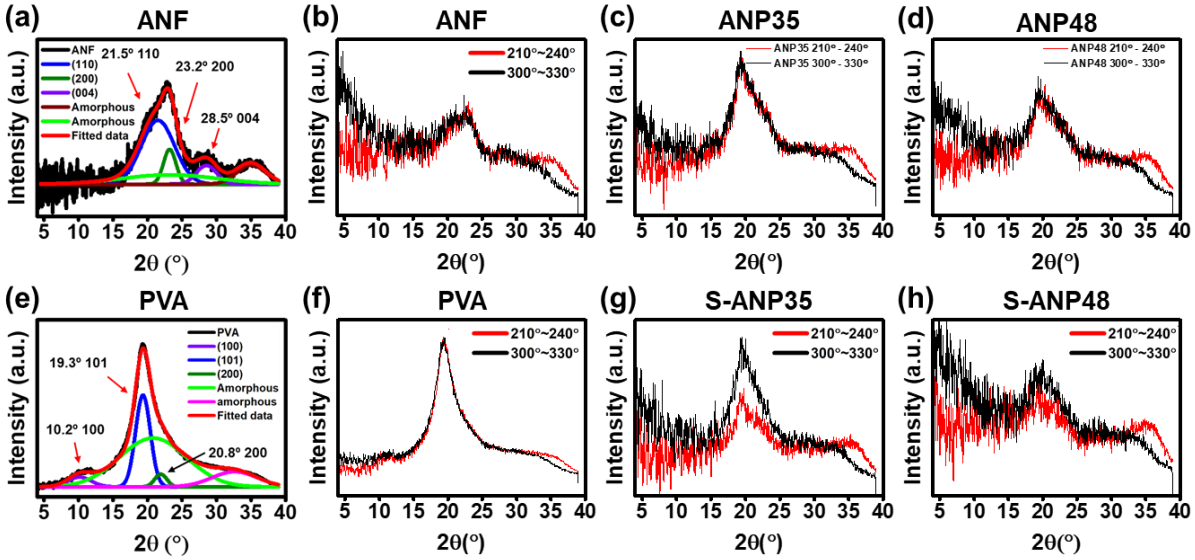

Figure S7. Deconvoluted WAXS scattering intensity profiles of (a) ANF and (e) PVA as a function of 2θ. (b-d and f-h) Scattering intensity profiles with the selected azimuthal angle regions of 210º ~ 240º and 300º ~ 330º for ANF, PVA, ANP and S-ANP samples.

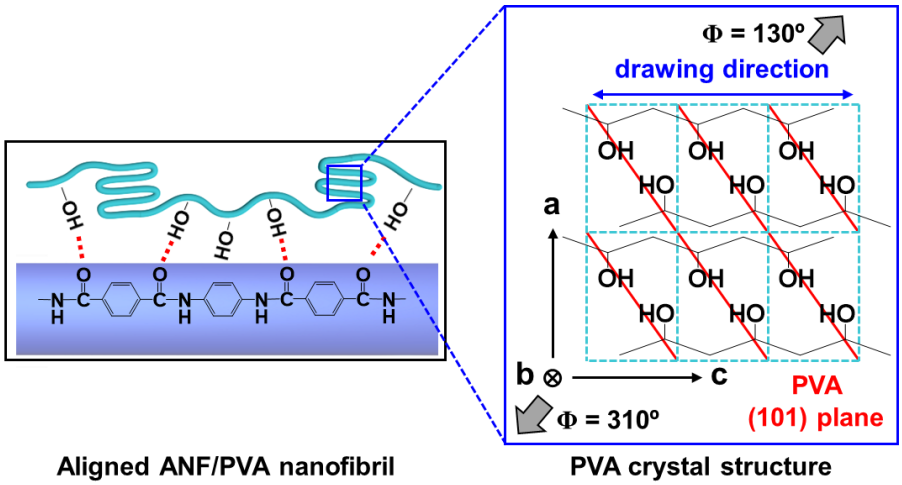

Figure S8. Schematic illustrations for the aligned ANF/PVA nanofibrils with PVA crystal domains. The (101) plane of PVA is oriented perpendicular to the azimuthal angle (Φ) of 130º and 310º direction.

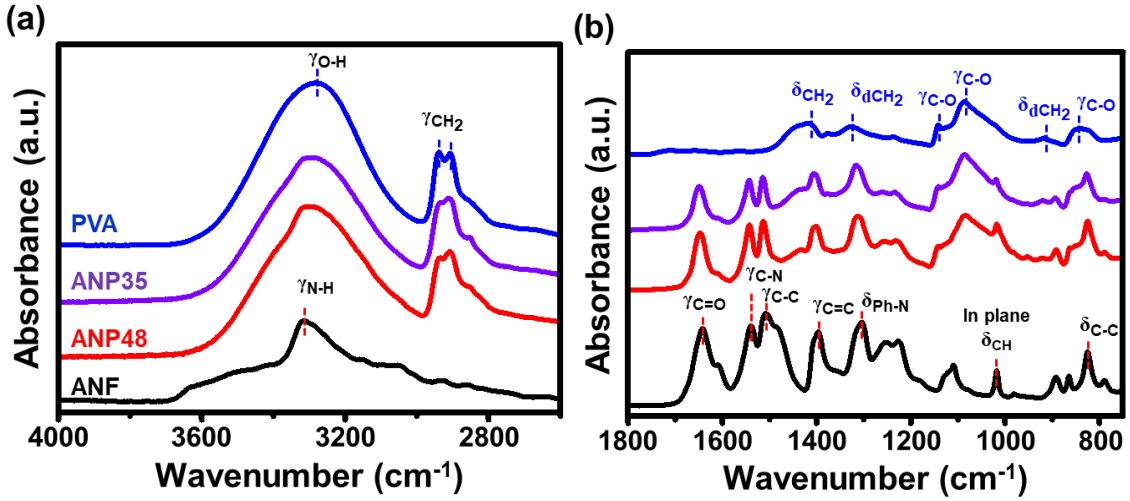

Figure S9. (a, b) FT-IR spectra of ANF, PVA, and ANF/PVA nanocomposites with different aramid volume fractions and peak assignments.

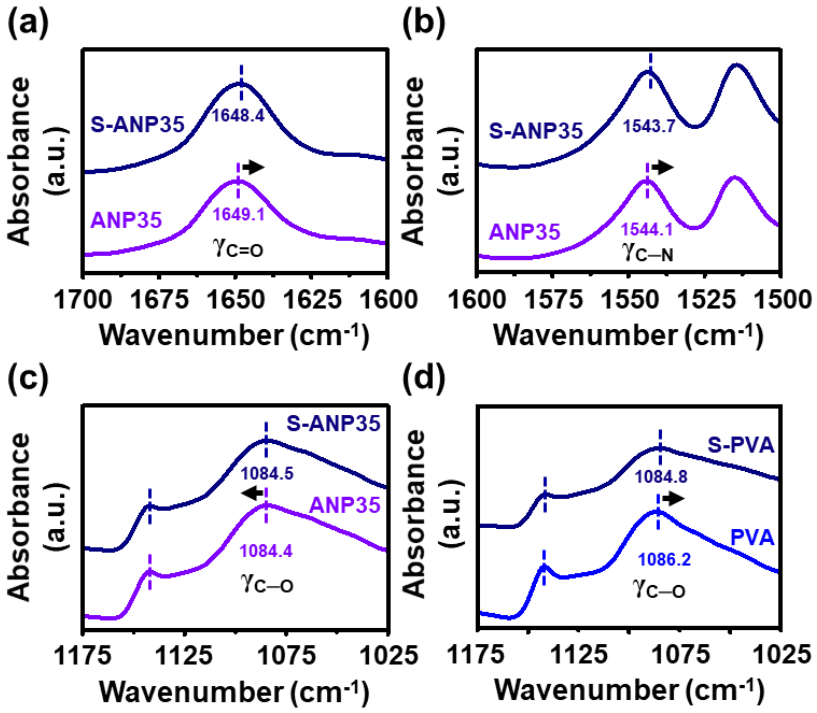

Figure S10. FT-IR spectra showing (a) C=O, (b) C–N, and (c) C–O stretching vibration modes for ANP35 and S-ANP35 samples and (d) PVA and S-PVA.

Deconvolution principles for dielectric loss spectra.

We adopted Havriliak-Negami function to deconvolute the dielectric loss spectra. Complex permittivity can be described as follows:

$$\varepsilon^* = \varepsilon' - i\varepsilon'' = -i\frac{\sigma}{\varepsilon_0\omega^s} + \sum_{j=1}^{n}(\varepsilon_{j\infty} + \frac{\Delta\varepsilon_j}{\left[1+(i\omega\tau_j)^{\alpha_j}\right]^{\beta_j}}) \quad (1)$$

The real part ε′ and imaginary part ε″ of the complex permittivity can be described as follows:

$$\varepsilon' = \varepsilon_\infty + \sum_{j=1}^{n}\Delta\varepsilon_j\left(1 + 2\left(w\tau_j\right)^{\alpha_j}\cos\left(\frac{\pi\alpha_j}{2}\right) + \left(w\tau_j\right)^{2\alpha_j}\right)^{-\beta_j/2}\cos\left(\beta_j\phi_j\right) \quad (2)$$

$$\varepsilon'' = \sum_{j=1}^{n}\Delta\varepsilon_j\left(1 + 2\left(w\tau_j\right)^{\alpha_j}\cos\left(\frac{\pi\alpha_j}{2}\right) + \left(w\tau_j\right)^{2\alpha_j}\right)^{-\beta_j/2}\sin\left(\beta_j\phi_j\right) + \frac{\sigma}{\varepsilon_0\omega^s} \quad (3)$$

$$\phi_j = acrtan\left(\frac{\left(w\tau_j\right)^{\alpha_j}\sin(\pi\alpha_j/2)}{1+\left(w\tau_j\right)^{\alpha_j}\cos(\pi\alpha_j/2)}\right) \quad (4)$$

where j is the number of each relaxation processes, $\Delta\varepsilon_j$ is the dielectric relaxation strength, τ_j is the relaxation time, and α_j and β_j are HN shape parameters ($0 < \alpha_j < 1$; $\beta_j < 1$) that characterize the symmetric and asymmetric broadening of the spectra, respectively. The term $i\frac{\sigma}{\varepsilon_0\omega^s}$ reveals the conductivity, where ε_0 is the permittivity of free space, σ is the dc conductivity, and s is a fractional exponent describing the conduction mechanisms. By designating α_j, β_j, τ_j, $\Delta\varepsilon_j$, $\frac{\sigma}{\varepsilon_0}$ and *s* as a fitting parameter, dielectric loss spectra were deconvoluted using equation 3. As can be seen in Figure S10, all dielectric loss spectra decreases exponentially upon increasing frequency, which can be assigned to the conductivity term. The broad shoulder can be assigned to the β relaxation of the ANFs and PVA. Pristine ANF and PVA were deconvoluted with a single relaxation term and single conductivity term and ANF/PVA composites were deconvoluted with two relaxation term and single conductivity term. To increase the accuracy of the deconvoluted spectra, each dielectric loss spectra was first fitted only with the conductivity term $\frac{\sigma}{\varepsilon_0}$ and *s* to find out initial parameter of conductivity term as the conductivity term is predominant in dielectric loss spectra. Then, spectra was fitted with conductivity term and relaxation term. Validity of each deconvoluted results was confirmed by the r^2 value of fitted results. The r^2 value of fitted results ranged from 0.9983 to 0.9999, indicating that results fit the original data.

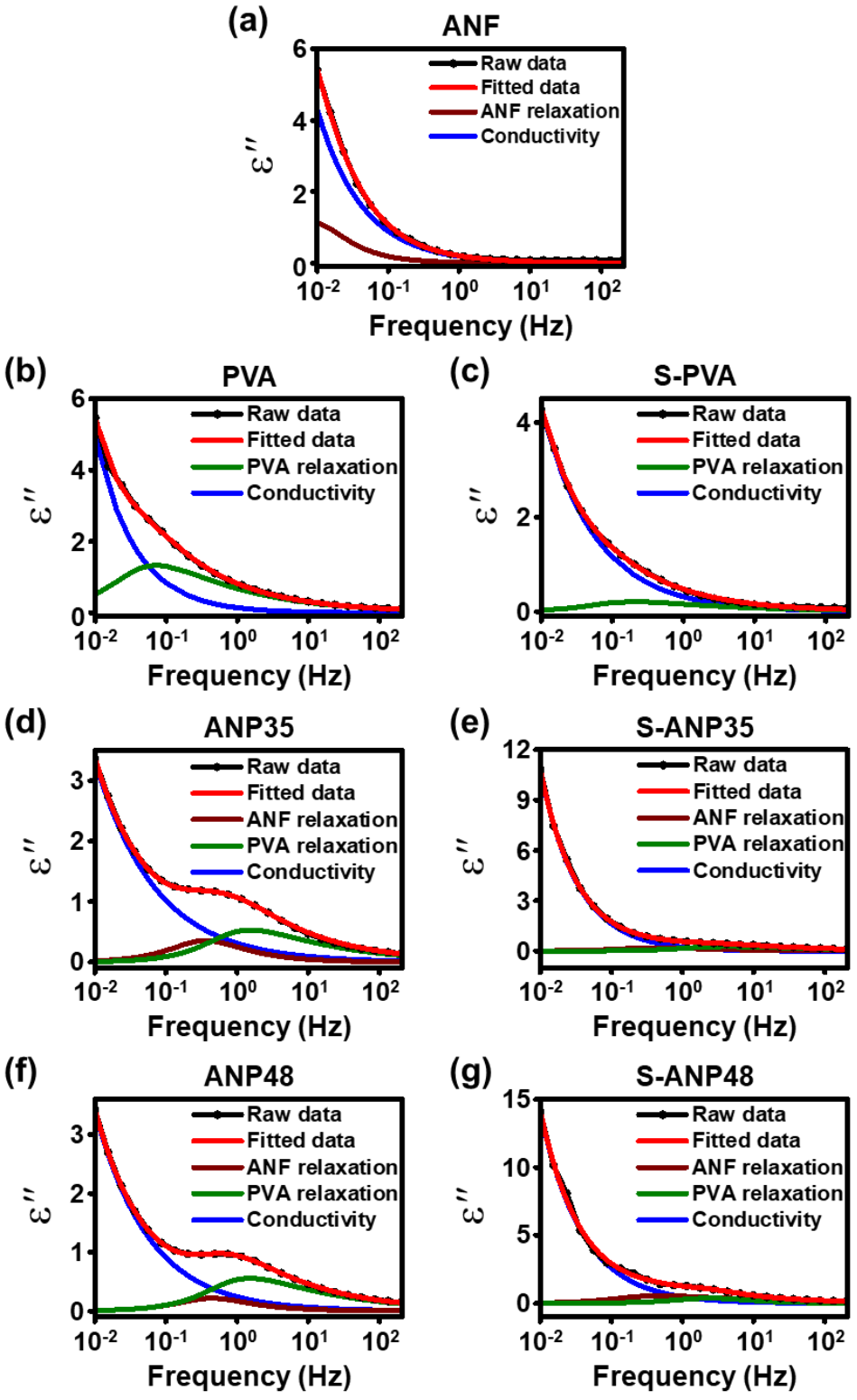

Figure S11. The fit results of HN functions to the dielectric loss spectra of (a) ANF, (b) PVA, (c) S-PVA, (d) ANP35, (e) S-ANP35, (f) ANP48, and (g) S-ANP48.

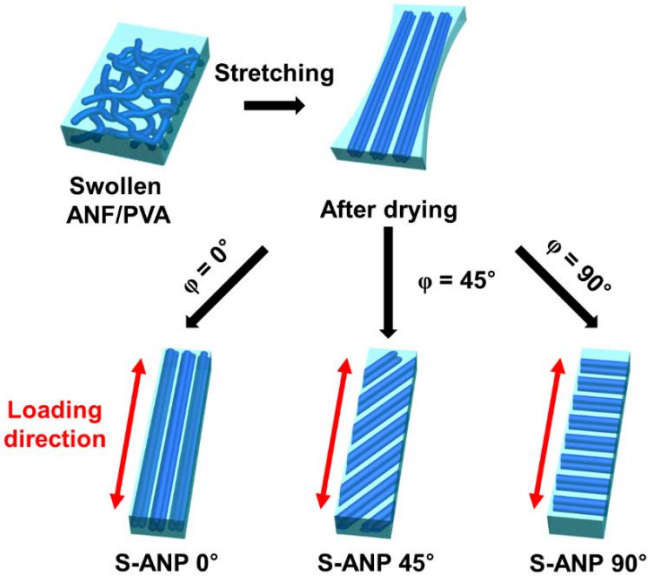

Figure S12. Schematics of the fabrication of highly aligned ANF/PVA nanocomposites and the preparation of ANF/PVA samples with certain fiber loading angles.

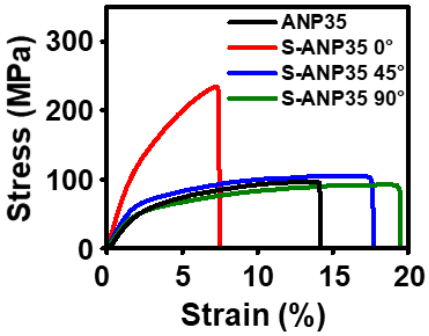

Figure S13. Tensile test results. Stress–strain curves for ANP35 and S-ANP35 with various loading angles relative to the strain directions.

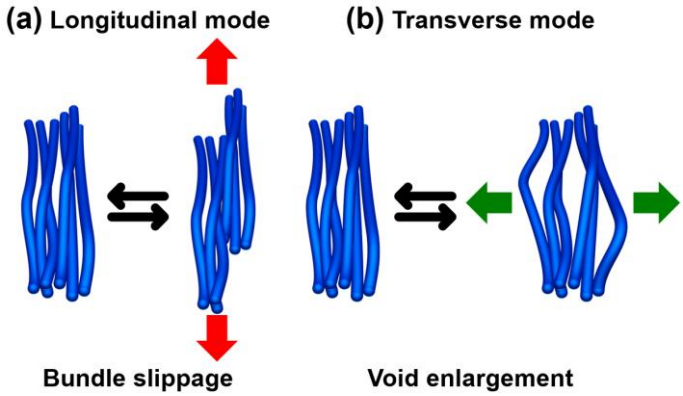

Figure S14. Schematics of the energy dissipation mechanisms in the aligned ANF/PVA nanofibrillar structures with dynamic strains in the (a) longitudinal and (b) transverse direction.

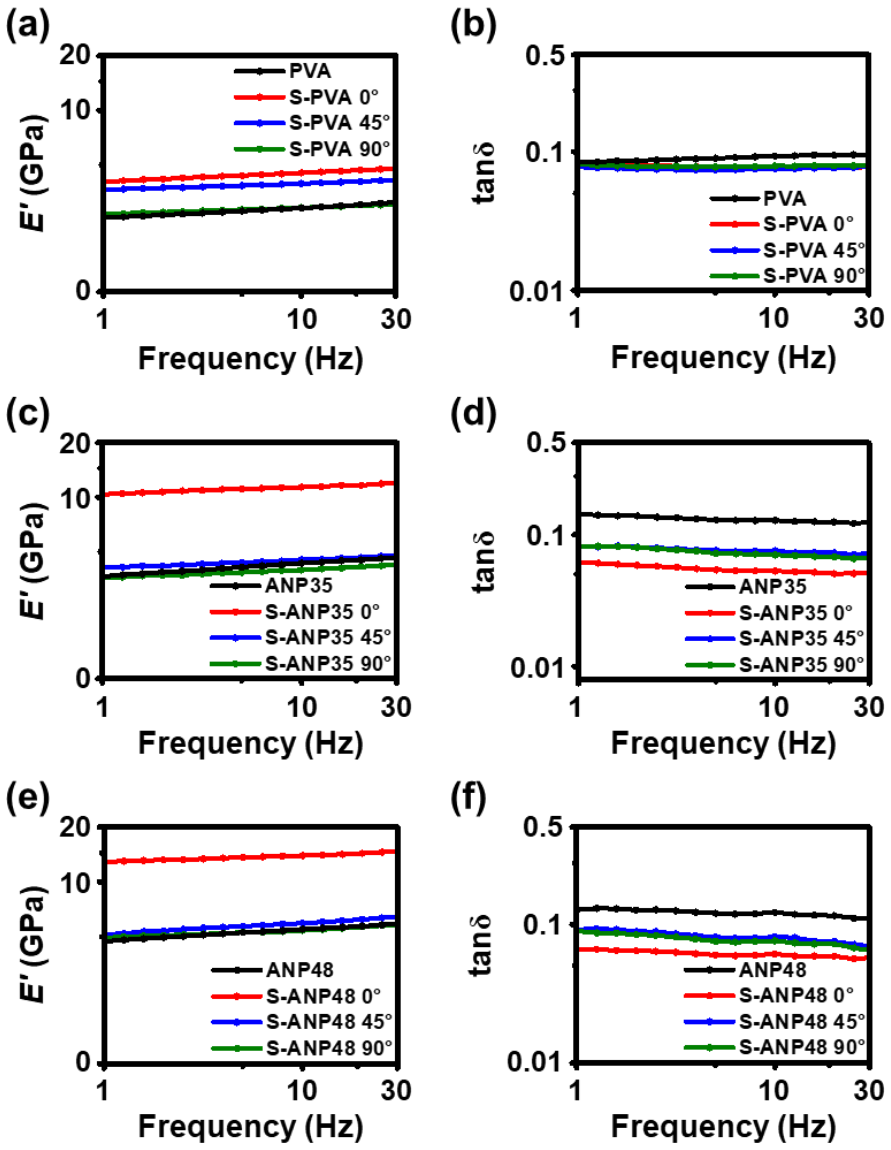

Figure S15. Storage moduli and tanδ of (a, b) PVA and S-PVA, (c, d) ANP35 and S-ANP35, (e, f) and ANP48 and S-ANP48.

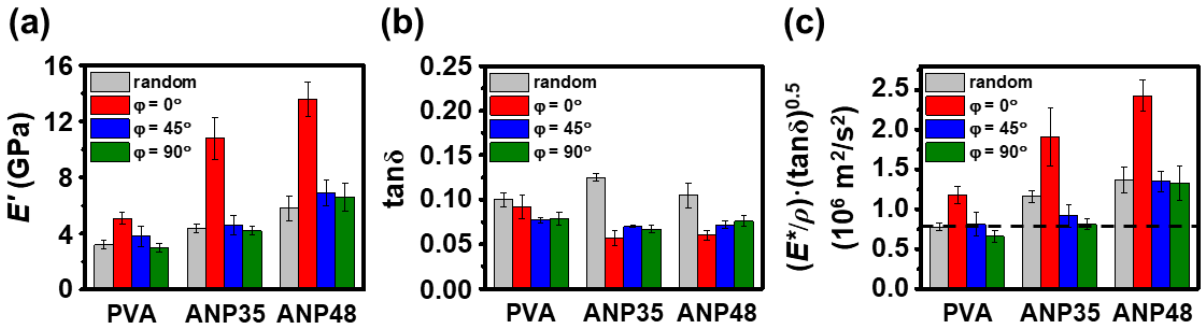

Figure S16. Dynamic mechanical analysis results of (a) storage moduli, (b) tanδ, and (c) $(E^*/\rho)\cdot(\tan\delta)^{0.5}$ of PVA and ANF/PVA nanocomposites obtained at 30 Hz with various loading angles.

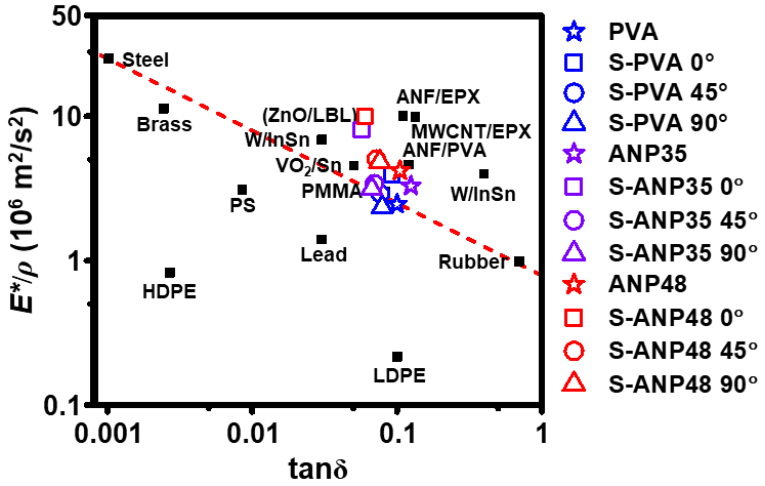

Figure S17. Summary plot of dynamic mechanical properties obtained at 30 Hz for PVA and ANF/PVA nanocomposite samples with various volume fractions and loading angles. Additional data is included for common materials and composites.

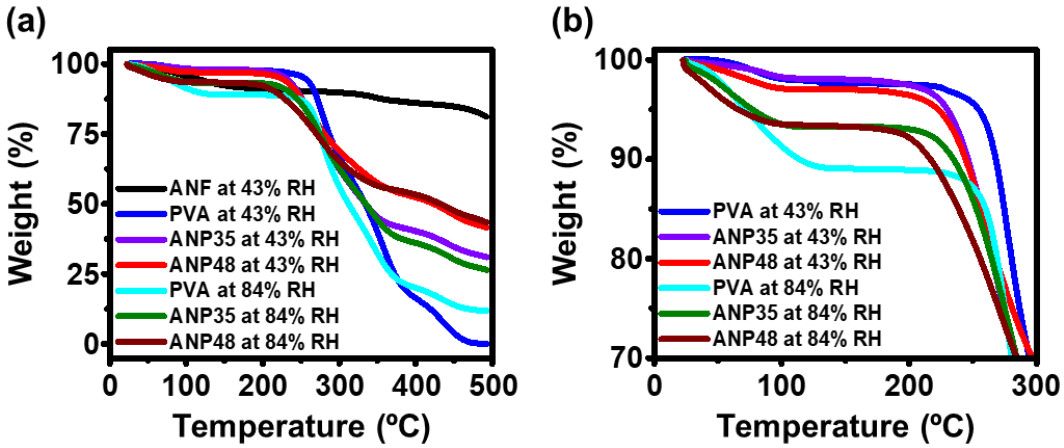

Figure S18. (a) Thermogravimetric analysis data for ANF, PVA, and ANF/PVA nanocomposites with 43% and 84% relative humidity conditions. (b) Enlarged spectra for 0-300 °C region.

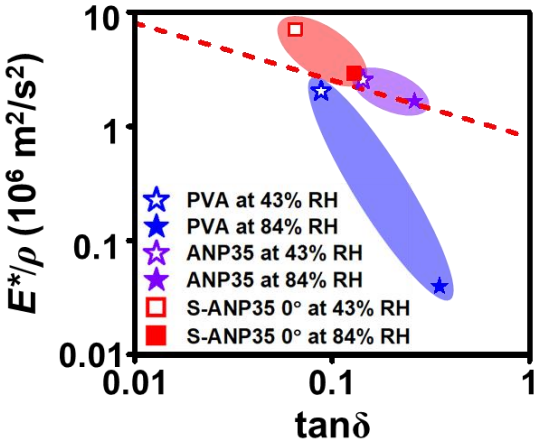

Figure S19. Summary plot of dynamic mechanical properties obtained at 1 Hz for PVA, ANP35 and S-ANP35 0º with different relative humidity conditions.